



Determination of permeation pathways of hydrophilic or hydrophobic dyes through the mammary papilla



Samantha L. Kurtz^{a,b}, Louise B. Lawson^{a,*}

^a Department of Microbiology and Immunology, Tulane University School of Medicine, New Orleans, LA 70112, USA

^b Bioinnovation Ph.D. Program, Tulane University School of Science and Engineering, New Orleans, LA 70118, USA

ARTICLE INFO

Keywords:

Transpapillary
Breast cancer
Nipple
Drug delivery
Lipophilic

ABSTRACT

The transport pathways and permeation kinetics of lipophilic and hydrophilic fluorescent dyes through porcine mammary papillae were visualized and quantified. Porcine mammary papillae, removed from full-thickness abdominal tissue, were positioned in a Franz diffusion cell for passive diffusion studies. Solutions containing the fluorescent dyes were applied topically for time periods ranging from 30 min to 48 h. Dye concentrations in tissue and Franz diffusion compartments were analyzed using fluorescence microscopy and fluorimetry. Fluorescence micrographs elucidated two permeation pathways, transepidermal and transductal. Hydrophilic sulforhodamine B predominantly penetrated via the transepidermal route, while lipophilic Nile red diffused mainly by the transductal route. An almost 4-fold higher amount of sulforhodamine B was retained within the nipple over time compared to Nile red, despite both dyes permeating through the tissue at similar rates. Diffusion through the porcine nipple was 500-fold higher than through adjacent skin for both dyes, likely attributable to the two mammary ducts which provide an entry point and transport route through the tissue. These results, generated from both qualitative and quantitative evidence at a micro and macro scale, demonstrate that the mammary ducts provide a direct pathway that contributes significantly to passive transport through the nipple, particularly for lipophilic molecules.

1. Introduction

Invasive breast cancer is the most frequently diagnosed cancer, with an estimated 250,000 women diagnosed annually (American Cancer Society, 2017). An additional 167,000 women will be diagnosed with high-risk, pre-malignant or non-invasive breast lesions, including atypical hyperplasia, lobular carcinoma in situ, and ductal carcinoma in situ (American Cancer Society, 2017; Hartmann et al., 2015). In the earliest stages, pre-malignant or malignant cells are localized within the ducts of the breast. Yet, the treatment approaches for these women are the same as those with invasive cancer and impose psychological detriments resulting from a life-altering, irreversible mastectomy or unnecessary systemic side effects as a result of oral treatments on women who may never develop invasive breast cancer. Moreover, the substantial side effects are a contributing factor in the low adoption and adherence rates of chemopreventive drugs. Only 16% of women identified as high-risk for developing breast cancer adopt primary preventive therapy and of those, < 65% complete the full 5-year regimen (Smith et al., 2016). Therefore, despite the availability of effective drugs, their systemic delivery route has limited their use in the

prophylactic setting.

A local drug delivery strategy, however, would maximize drug exposure within the breast, while minimizing systemic exposure, thereby resolving the primary issue of side effects while still reaping the benefits of a preventive treatment. A variety of approaches have been suggested to localize drug exposure within the breast, including transdermal, intraductal and, of our particular interest, transpapillary drug delivery.

Traditional transdermal drug delivery involves application of a patch or gel on the surface of breast tissue. This passive technique achieves similar breast tissue drug concentrations compared to oral treatment, 5-fold reduced plasma concentrations, and extended retention of drug compared to other application sites, thus validating local treatment as a non-toxic treatment alternative (Lee et al., 2014, 2015). However, due to the tight, ordered packing of the stratum corneum, this technique is limited to small, lipophilic compounds that are able to efficiently traverse the skin's innate barrier. Furthermore, this delivery technique is not highly localized within the mammary ductal network. The drug primarily exposes the epidermis and underlying fatty tissue rather than the mammary duct epithelium, which is the origin of a vast majority of breast cancers (American Cancer Society, 2016).

* Corresponding author at: Department of Microbiology and Immunology, Tulane University School of Medicine, 1430 Tulane Ave (8638), New Orleans, LA 70112, USA.
E-mail address: lbraud@tulane.edu (L.B. Lawson).

The first proposed highly localized method was intraductal drug delivery, whereby a small catheter is used to inject a drug solution into mammary duct orifices. Clinical studies confirm the feasibility of repeated identification, cannulation, and injection of the mammary duct orifices, as well as exposure of the entire length of the mammary duct to the injected solution (Love and Barsky, 2004; Love et al., 2013). However, a local anesthetic and a trained surgical professional would be required for administration, leading to questions of practicality for wide-spread adoption, particularly for long-term treatment regimens, and the possibility of self-administration.

A second highly localized strategy, transpapillary drug delivery, offers a non-invasive approach that capitalizes on the mammary ducts to serve as an entry point, conduit, and reservoir. Although previous studies have established the feasibility of permeation through the nipple (Dave et al., 2014; Davison, 2008; Lee et al., 2010), the associated permeation kinetics and cumulative amount of drug permeated vary. While one study contends that equilibrium is reached after 6 h (Lee et al., 2010), others suggest continued permeation for 48 h (Dave et al., 2014, 2016). Furthermore, the total accumulation of molecules and concomitant permeation parameters differ over 200-fold (Alsharif et al., 2017; Dave et al., 2014, 2016). A molecule's physicochemical properties may explain, in part, the extreme kinetic variation, as well as the utilization of transport pathways. Lipophilicity has previously been associated with localization around the mammary duct, while hydrophilic molecules are more likely to diffuse throughout the tissue in an unrestricted manner (Dave et al., 2014), insinuating varied use of transport pathways. However, alternative permeation routes beyond the ductal network have yet to be addressed nor have any permeation pathways been quantified.

The objective of this study was to visualize and quantify the permeation routes and establish the permeation kinetics through the mammary papilla. Two fluorescent dyes, Nile red (NR) and sulforhodamine B (SRB), were chosen as model lipophilic and hydrophilic molecules, respectively. These model dyes allowed us to determine the influence of lipophilicity due to their similar molecular weight (MW) (MW = 318.3 and 558.6 Da for NR and SRB, respectively) but differing lipophilicity. A common indicator of lipophilicity is a molecule's octanol-water partition coefficient, or logP (Mannhold et al., 2009). The logP value for NR is 5 (Kuchler et al., 2009) while SRB is -2 (Amato et al., 2017). These dyes are also relevant models for therapeutic and chemopreventive drugs used clinically in breast cancer treatment and prevention. Tamoxifen (MW = 371.5 Da; LogP = 7.1 (Kim et al., 2016)) and raloxifene (MW = 473.5 Da; LogP = 5.4 (Kim et al., 2016)) are both lipophilic drugs, making NR an appropriate model, while 5-fluorouracil (MW = 130.1 Da; LogP = -0.89 (Kim et al., 2016)) is a hydrophilic drug, similar to SRB. Furthermore, we compared transpapillary to transdermal administration to establish the contribution of mammary ducts to total permeation by assessing differences in transport kinetics between the two routes of delivery.

2. Materials and methods

2.1. Materials

Acetone, Cytoseal60, ethanol, isoamyl alcohol, NR, phosphate-buffered saline (PBS), and SRB were purchased from ThermoFisher. Biosol was purchased from National Diagnostics. All chemicals were used as supplied without further purification. Strips of full thickness porcine abdominal tissue were supplied by a local market and stored at -20°C prior to use.

2.2. Tissue preparation

Upon use, the nipple or adjacent skin was thawed and dermal fat was mechanically removed. A digital caliper (Traceable Digital Caliper) was used to measure the thickness of each tissue specimen, which was

then mounted on a jacketed Franz diffusion cell (surface area 0.64 cm^2 ; PermeGear).

2.3. Fluorescent dye solution preparation

Two fluorescent dyes, NR and SRB, were used as model lipophilic and hydrophilic molecules, respectively. Each dye was used at a 3.14 mM concentration. Because of solubility differences, NR was solubilized in pure ethanol, while SRB was solubilized in a solution of ethanol:PBS at a 1:1 (vol:vol) ratio.

2.4. In vitro diffusion studies

To examine the kinetics of dye diffusion into and through the mammary papillae or skin, the receiver compartment of a Franz diffusion cell was filled with 5 mL of the compatible solvent for each dye (ethanol for NR and 1:1 ethanol:PBS (vol:vol) for SRB) unless otherwise indicated. These solvents were chosen for consistent partitioning from the donor compartment to the tissue and from the tissue to the receiver compartment. This volume was sufficient to ensure direct contact between the tissue and receiver compartment solution. The diffusion cell was maintained at 37°C with continuous stirring of the receiver compartment. The donor compartment was filled with $300\ \mu\text{L}$ of 3.14 mM NR or SRB in solution and left in contact with the tissue samples for a time period ranging from 30 min to 48 h. At the specified end-point, the donor chamber contents and tissue were removed and the tissue surface was washed three times with 1 mL of the compatible solvent for further processing.

2.5. Tissue Imaging by fluorescence microscopy

Nipples were stored in OCT (Tissue-Tek) and frozen at -80°C . A cryostat (Leica CM1860) was used to coronally section the nipple from tip to base. At 1-mm intervals, three $10\text{--}20\ \mu\text{m}$ sections were collected and mounted on a slide, incubated at 37°C for 6 h, and sealed using Cytoseal 60. Fluorescence micrographs of the entire tissue section were obtained using a Zeiss Axioplan 2 with a Cy3 filter set (Chroma HQ 41007: HQ 710/75, HQ 515/30, Q 570 LP) at 10x magnification. For each dye, images were taken at the same exposure to minimize variation associated with image data. Images were then compiled using SlideBook 6 Software (Intelligent Imaging Solutions) to create a montage of the entire nipple cross section.

2.6. Generation of fluorescence intensity profile

The plot profile tool in ImageJ software (Schneider et al., 2012) was used to calculate the fluorescence intensity as a function of radial distance across the section. All analysis was performed on images of coronal nipple cross sections from a depth of 1 mm from the tip of the nipple. Each image was subject to eight to ten regions of interest, which were then averaged to generate one intensity profile per tissue section. The region of interest lines were drawn either normal to the tissue edge or normal to the mammary duct towards the inner dermis, generating quantitative fluorescence intensity profiles in the x-y plane.

2.7. In vitro penetration study

Porcine nipples were positioned in the Franz diffusion cell for 30 min to 48 h. Following permeation, the tissue was cut into small pieces with scissors or sectioned on a cryostat (Leica CM1860). When a cryostat was used to cut the tissue, nipples were coronally sectioned in $100\ \mu\text{m}$ increments from tip to base. Tissue sections were collected in 1 mm increments into sample tubes until the tissue was completely sectioned. The weight of sample tubes were recorded pre-and post-addition of tissue to calculate the weight of individual tissue sections. Once the tissue was in small pieces, the dye was extracted from tissue

using 6:1 isoamyl alcohol:acetone (vol:vol) with vortexing for samples treated with NR or SRB-treated specimens were solubilized in Biosol for at least 3 h. For each sample, 100 μ l of the fluorescent solution was plated in duplicate in a black-walled, 96-well flat-bottomed plate. The concentration of each sample was determined using a fluorimeter (Synergy H1 microplate reader) at excitation/emission 560/590 for SRB and 550/630 for NR by interpolating from a calibration curve.

2.8. *In vitro* permeation study

Porcine nipples or adjacent tissue was positioned in the Franz diffusion cell for 8 to 48 h. Every 8 h, a 300 μ l sample was collected from the receiver chamber and replaced with fresh ethanol for NR or 1:1 PBS:ethanol (vol:vol) for SRB. The fluorescence from each sample was measured using fluorimetry in the same manner as in the *in vitro* penetration study detailed above.

2.9. Permeation parameter calculations

The steady-state portion (24–48 h) of the permeation profile was used to calculate the flux (J) from the slope, and lag time (t_{lag}) from the x-intercept using linear extrapolation. The permeability coefficient (P) was calculated from flux (J) using the equation, $P = J/C_d$, where C_d is the concentration in the donor compartment (3.14 mM) and was assumed constant. The diffusion coefficient (D) was calculated from lag time (t_{lag}) using the equation, $D = L^2/6t_{lag}$, where L is the tissue height. The partition parameter (K) was calculated from the permeability (P) and diffusion coefficients (D) using the equation $K = PL/D$ (Mohd et al., 2016). Furthermore, each transport property is reported as a relative difference, which is the ratio of the transport property through the nipple divided by the skin.

2.10. Statistical analysis

GraphPad software was used in all statistical analysis. For the *in vitro* penetration study (2.7), multiple t-tests (GraphPad software) were used to compare the retention of each dye at individual time points. For the *in vitro* permeation study and permeation parameter calculations (2.8 & 2.9), an ordinary one-way ANOVA was used with Sidak's multiple comparisons test to make the following comparisons: NR nipple vs SRB nipple, NR skin vs SRB skin, NR nipple vs NR skin, SRB nipple vs SRB skin. All results were deemed significant at $p < 0.05$.

3. Results and discussion

3.1. Visualization of transport pathways through the nipple

The fluorescent dyes used in our studies were selected because of their similar molecular weight (NR MW = 318.37 Da and SRB MW = 558.6 Da) but differing lipophilicity (Fig. 1). With a log P value of 5, NR is highly lipophilic (Kuchler et al., 2009) as compared to SRB, which has a log P value of -2 (Amato et al., 2017). The use of these two fluorescent dyes allowed us to establish the role of molecular hydrophilicity on permeation into and through the mammary papillae.

To better understand the pathways by which the model hydrophilic and lipophilic dyes permeate into and through the mammary papillae, porcine nipples were treated with 3.14 mM solutions of either NR or SRB for various times. After cryo-preservation, coronal cross sections were collected at a depth of 1 mm from the tip of the nipple. The spatial distribution of the hydrophilic and lipophilic fluorescent dyes within the porcine nipple was then analyzed using fluorescence micrographs of the tissue.

3.1.1. Qualitative mapping of dye permeation

To qualitatively illustrate the spatial distribution of hydrophilic and lipophilic fluorescent dyes within the porcine nipple over time, entire

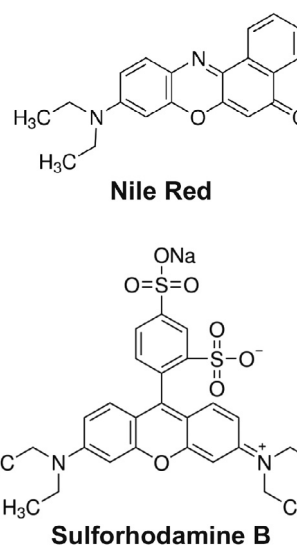


Fig. 1. Chemical structures of fluorescent molecules used in present study (Greenspan and Fowler, 1985; Yan et al., 2009).

coronal cross sections of the nipple were analyzed. Each image is from a depth of 1 mm from the nipples tip. Representative fluorescence micrographs are shown in Fig. 2. The white arrows indicate the mammary ducts. Porcine tissue was used as a surrogate for human tissue as previous studies indicate their chemical and structural similarities (Dave et al., 2014).

Fig. 2(a–c) provides the localization of the lipophilic dye NR within the porcine nipple over time ranging from 30 min to 8 h. After 30 min, NR is observed within the outer epidermis and the outer edge of the mammary ducts. However, there is limited fluorescence within the dermis. After 3 and 8 h, NR penetrated slightly further beyond the epidermis and mammary ducts, yet the majority of the dermis remains free of fluorescence. Fig. 2(d–f) indicates the localization of the hydrophilic dye SRB within the porcine nipple over time ranging from 30 min to 8 h. After 30 min, SRB is detected within the outer epidermis and the outer edge of the mammary duct with a distribution similar to the lipophilic dye. However, after 3 and 8 h, the entire nipple cross section displays detectable fluorescence, indicating the propensity of SRB to further diffuse into the dermis. These results are consistent with previous reports of lipophilic NR localizing in and around the mammary duct, while hydrophilic SRB was uniformly distributed throughout the tissue after 12 h of treatment (Dave et al., 2014), despite the different solvents and dye concentrations used by Dave and coworkers.

As evidenced by the fluorescence micrographs, the two penetration routes into and through the nipple are via the stratum corneum (transepidermal) or the mammary ducts (transductal). Both the hydrophilic and lipophilic model fluorescent dyes penetrated the nipple via both routes, as indicated by fluorescence surrounding the epidermis and mammary ducts after only 30 min. However, the propensity to which each dye diffuses via these transport pathways is different, as evidenced by complete saturation of the dermis by the hydrophilic dye, but not the lipophilic dye, at the longer time points.

3.1.2. Quantitative comparison of dye distribution within coronally-sectioned tissue over time

While the qualitative assessment of fluorescence micrographs provided insight into the permeation pathways of each dye, a quantitative analysis provides a more thorough insight regarding the diffusion of the model dye molecules into and through the tissue. All analysis was performed on coronal cross sections at a depth of 1 mm from the tip of the nipple. Image analysis software was used to plot the fluorescence intensity as a function of distance radially inward from the outer edge

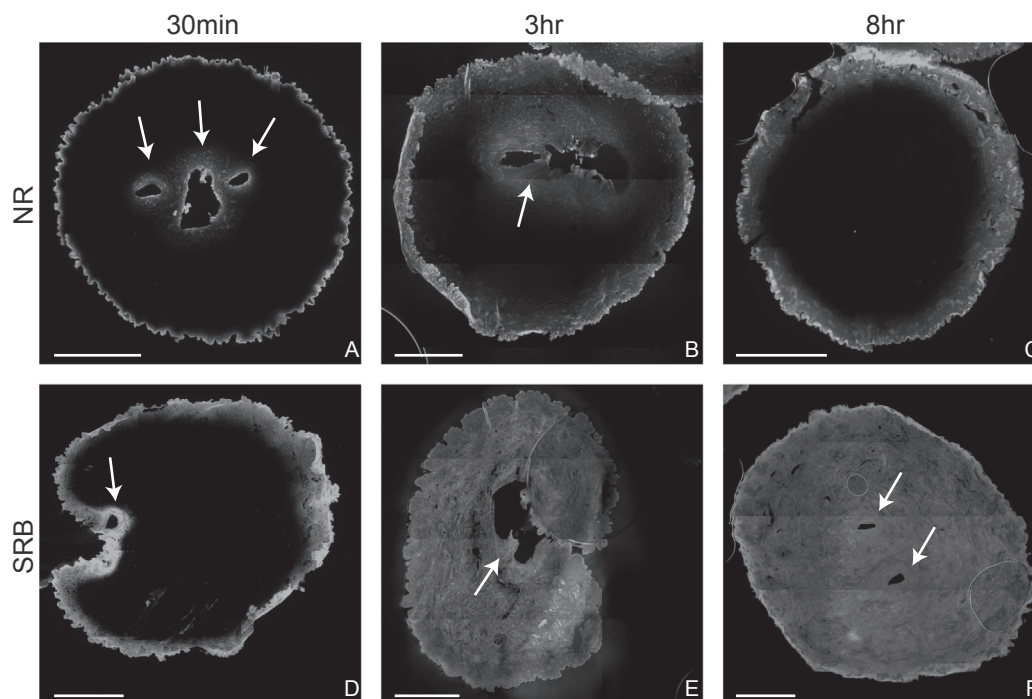


Fig. 2. Representative fluorescence micrographs of porcine nipple cross sections following diffusion of NR (A–C) or SRB (D–F) for 30 min (A and D), 3 h (B and E), or 8 h (C and F). All micrographs include coronal sections collected at a depth of 1 mm from the tip of the nipple. Scale bar indicates 1 mm.

or outward from the mammary duct, as indicated in Fig. 3. The fluorescent intensity profiles were then interpreted to evaluate the concentration gradient (slope) and tissue-solvent partition coefficient (y -intercept) (Yu et al., 2001).

After 30 min, hydrophilic SRB penetrated approximately 0.6 mm transepidermally and only 0.25 mm transductally, suggesting SRB predominantly enters the tissue via the transepidermal route. After 3 h, SRB diffused over 1 mm into the dermis of the nipple from both the outer edge of the tissue and duct. The shape of the fluorescent intensity profile at 3 h is maintained at 8 h, suggesting saturation within these tissue regions after just 3 h. However, lipophilic NR penetrated only 0.2 mm transepidermally and 0.25 mm transductally, after 30 min, suggesting NR predominantly enters the tissue via the transductal route. After 3 and 8 h, NR continues to diffuse through the tissue reaching 0.5 mm and over 1 mm from the epidermis and duct, respectively. Furthermore, the overall NR fluorescence within the dermis after 8 h was much lower as compared to SRB, indicating that a greater amount of SRB is permeating into the tissue than NR.

In addition to penetration distance, the concentration gradients were calculated for Fig. 3 from the stratum corneum to the dermis and the duct to the dermis. The slope, 95% CI, and r^2 corresponding to the linear regression is reported in Table 1. As expected, the concentration gradients decreased over time for both dyes from both the transepidermal and transductal directions, indicating progression towards equilibrium. Transepidermally, the concentration gradients remained steeper for NR compared to SRB. However, transductally, the concentration gradient was only steeper for NR at the earliest time point (30 min), but quickly leveled-off to a value lower than SRB. This can likely be explained by the limited diffusivity of NR through the epidermis, which has a thickness of 45 to 90 μm in the human nipple (Kolliker, 2015) and is likely comparable for the porcine nipple. Additionally, this is further supported by the decrease in partition coefficient (y -intercept) from the transductal direction over time, but not from the transepidermal direction, for NR.

3.2. Influence of lipophilicity on transpapillary disposition kinetics

In our initial studies detailed in Section 3.1 above, the distribution of dye was assessed at a single depth of 1 mm from the tip of the nipple. To give a macro-scale assessment of distribution within the whole tissue, dye retention both in the tissue specimen as a whole and at varying depths along the tissue thickness was analyzed. As expected based on the differences in distribution patterns noted in the fluorescence micrographs for NR and SRB, the permeation kinetics throughout the tissue were significantly different between the model hydrophilic and lipophilic molecules (Fig. 4). Hydrophilic SRB quickly penetrated the nipple before reaching a saturation point of approximately 190 μg after 24 h. However, lipophilic NR slowly penetrated the nipple over time, retaining only 50 μg after 48 h without reaching a saturation point. Lee et al. indicated comparable penetration results for a small, lipophilic molecule (Lee et al., 2010). They reported no penetration difference between 6- and 48-h application times for PD98059, which has a LogP value of 2.9 (Kim et al., 2016). This slow kinetic profile similar to NR is likely attributable to the lipophilic nature of the two molecules.

In assessing dye concentration as a function of tissue depth, majority of the dye was retained within the first millimeter of tissue (Fig. 5). As tissue depth increases, the concentration of dye decreases. As expected from the disposition kinetics of the whole nipple, the kinetics of dye disposition by depth also varies by lipophilicity. Between 30 min and 24 h, the concentration of SRB increased at each tissue depth (Fig. 5). The most drastic increase was found in the tip of the nipple, while the concentration increase with time was less apparent within the deeper regions of the tissue. However, the concentration of NR did not change with time at depths of 1 mm or more. These results are consistent with the quantitative image analysis presented in Section 3.1.2. Due to the 3-dimensional trapezoidal shape of the nipple, the donor solution is in contact with the stratum corneum at all tissue depths (1–7 mm) and therefore penetration via the transepidermal route occurs at depths beyond the tip of the nipple. Because the hydrophilic SRB is more likely to permeate the mammary papillae's transepidermal route, it was able to permeate into the nipple at depths beyond 1 mm. The lipophilic NR

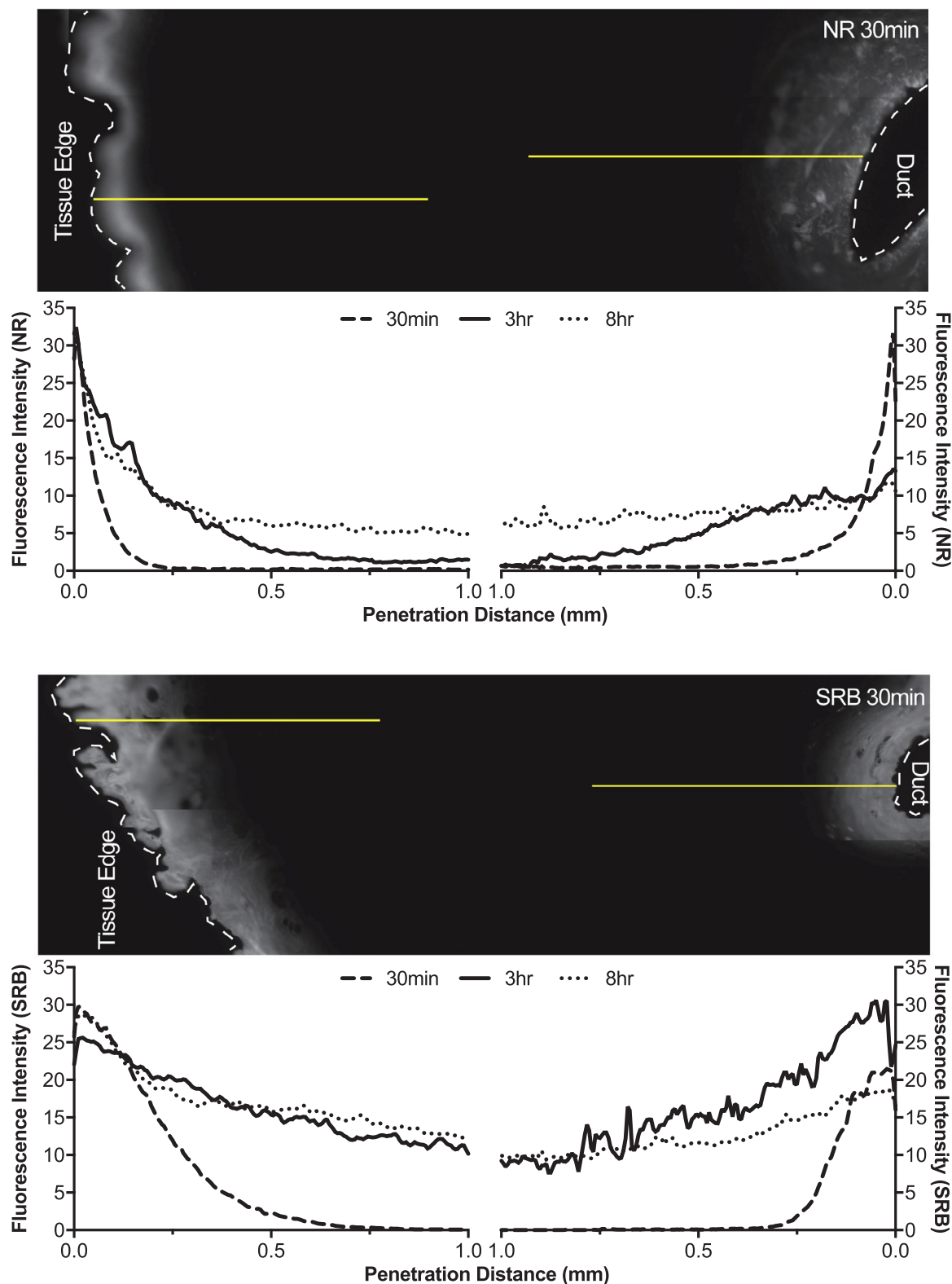


Fig. 3. Representative micrographs and corresponding fluorescence intensity profiles of NR (top) or SRB (bottom) as a function of penetration distance following 30 min, 3 h or 8 h permeation. Yellow lines in micrograph images are 1 mm in length. Each curve is an average of eight to ten regions of interest per tissue section (n = 1–4). (For interpretation of the references to colour in this figure legend, the reader is referred to the web version of this article.)

minimally penetrated to these tissue depths due to its limited transepidermal transport.

For the *in vitro* diffusion experiments detailed above, the solvents used for SRB and NR were 50% ethanol in PBS and 100% ethanol,

respectively. In previous studies, we have shown that ethanol increases skin permeability (Jaimes-Lizcano et al., 2011) and that long-term hydration alters stratum corneum microstructure, which can also enhance molecular transport into the skin (Tan et al., 2010). Therefore, to

Table 1

Linear regression results for the fluorescence intensity profiles for NR or SRB permeating through porcine nipple after 30 min, 3 h, or 8 h.

	NR		r^2	SRB		r^2
	Slope	95% CI		Slope	95% CI	
<i>Transepidermal</i>						
30 min	-264.20	-299.2 to -229.2	0.941	-73.25	-77.81 to -68.69	0.959
3 h	-83.51	-89.94 to -77.07	0.938	-23.03	-25.91 to -20.16	0.853
8 h	-69.91	-78.8 to -61.01	0.854	-48.03	-51.37 to -44.69	0.949
<i>Transductal</i>						
30 min	-243.30	-274.3 to -212.4	0.942	-88.84	-96.72 to -80.96	0.920
3 h	-11.18	-14.74 to -7.622	0.471	-34.35	-43.72 to -24.98	0.548
8 h	-11.48	-14.03 to -8.926	0.646	-16.13	-18.45 to -13.81	0.813

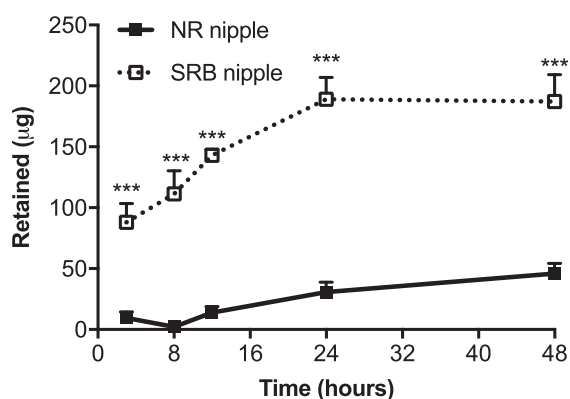


Fig. 4. Retention of NR or SRB within porcine mammary papilla following *in vitro* permeation for 3–48 h. Each point indicates mean + SEM (n = 4–10). *** indicates $p < 0.001$.

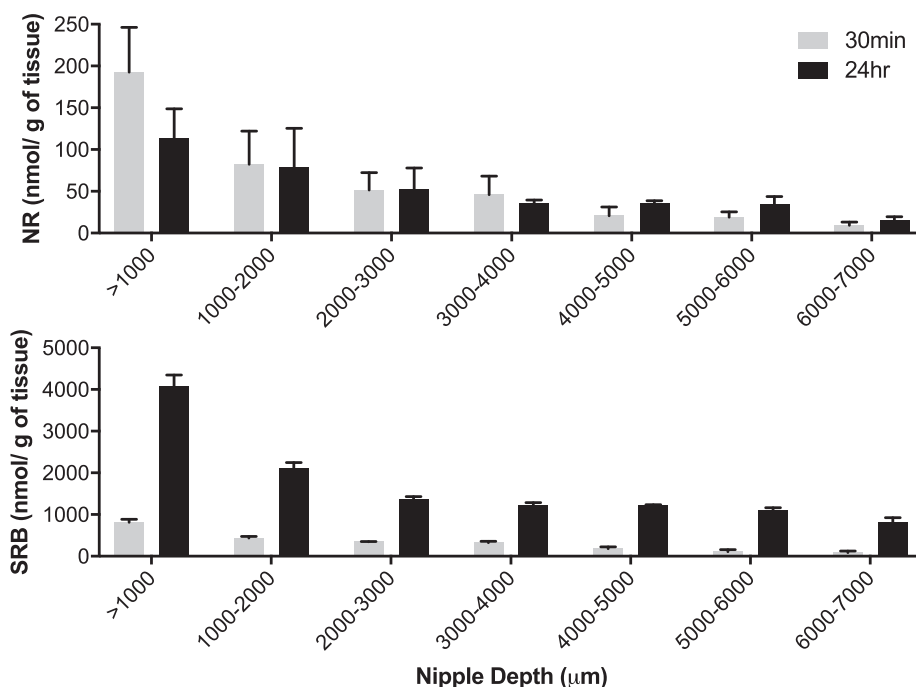


Fig. 5. Retention of NR (top) or SRB (bottom) after 30 min (gray bars) or 24 h (black bars) as a function of nipple depth. Each bar indicates mean + SEM (n = 3–7). (For interpretation of the references to colour in this figure legend, the reader is referred to the web version of this article.)

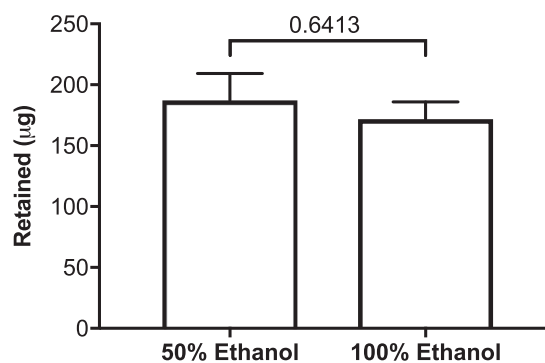


Fig. 6. Amount of SRB retained within porcine mammary papilla following *in vitro* permeation for 48 h when solubilized in either 50% ethanol or 100% ethanol. Each bar indicates mean + SEM (n = 3–5).

ensure the differences in disposition kinetics were not attributable to the solvents used for each dye, SRB was solubilized in 100% ethanol at the same concentration as in previous experiments, 3.14 mM. Fig. 6 indicates that there is no difference in the amount of SRB retained within the tissue after 48 h when solubilized in either 50% ethanol or 100% ethanol, supporting our conclusion that the disposition difference between the hydrophilic and lipophilic fluorescent molecules is due to the differences in the intrinsic physicochemical properties of each dye. This is consistent with a previous study that reports no significant change in penetration for 0–66% ethanolic solvents when the solution is unsaturated (Alsharif et al., 2017).

3.3. Influence of lipophilicity on transpapillary permeation kinetics

In addition to the disposition kinetics, which represent the retention of dye within the tissue, permeation kinetics were also compared for each fluorescent dye. These values characterize the amount of dye that permeates through the entire nipple thickness into the receiver compartment. Sink conditions were maintained, as indicated by receiver compartment concentrations < 1% that of the donor compartment after 48 h and therefore well below the saturation limit. As seen in Fig. 7,

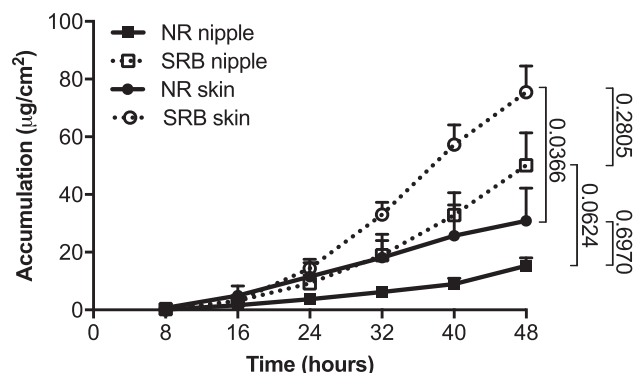


Fig. 7. *In vitro* permeation profiles of NR and SRB through porcine nipple or adjacent skin. Each point indicates mean + SEM (n = 3–4).

both molecules continuously permeated for 48 h through the nipple, consistent with the results from many published reports (Dave et al., 2014, 2016). Hydrophilic SRB permeated faster through the nipple than lipophilic NR, reaching a total accumulation of 50 $\mu\text{g}/\text{cm}^2$ compared to only 15 $\mu\text{g}/\text{cm}^2$, respectively, although these values were not statistically significantly different. Our reported accumulation is within the same range as permeation of 4-hydroxytamoxifen (5–20 $\mu\text{g}/\text{cm}^2$) after 48 h, but over 10-fold lower compared to permeation of estradiol (565–570 $\mu\text{g}/\text{cm}^2$) and 5-fluorouracil (690–1,050 $\mu\text{g}/\text{cm}^2$) (Alsharif et al., 2017; Dave et al., 2014). Anatomical differences may be responsible for this variation, as tissue samples in these and our studies were sourced from various suppliers without controlling for animal age or other factors, and the corresponding tissue height is unknown. Additionally, our lower accumulation could, in part, be attributed to the presence of keratin plugs. While we recognize that keratin plugs can impede permeation across the nipple (Dave et al., 2014), we did not intentionally remove the keratin plugs. However, considering a wipe of 70% ethanol is sufficient to remove them, it is possible they were dislodged during tissue preparation or dissolved upon exposure to ethanol (either a 50% or 100% solution). If the keratin plugs remained intact, the accumulated dye is likely underestimated approximately 30–50% in porcine tissue, which is based on the comparison of permeation with and without the keratin plug by Dave and coworkers (Dave et al., 2014). Furthermore, the accumulation values reported here are likely an underestimate of what would be expected in humans, due to anatomical differences between porcine and human mammary papillae. Human nipples have 5–9 ductal orifices (Love and Barsky, 2004), while porcine only have 2 (Martineau et al., 2012); therefore, permeation through the human nipple would be expected to be higher due to the larger number of direct shunts through the tissue.

The associated permeation parameters were calculated based on the

permeation kinetic curve and the results are reported in Table 2, along with the r^2 values corresponding to the linear regression. The linear portion of the curves (24–48 h) conformed to Fick's second law of diffusion, exhibiting r^2 values > 0.90. The results indicated that only one permeation parameter, flux (J), was significantly different between NR and SRB. The mean flux of SRB ($1.71 \pm 0.35 \mu\text{g cm}^{-2} \text{h}^{-1}$) through the nipple was significantly higher ($p = 0.023$) than that of NR ($0.47 \pm 0.11 \mu\text{g cm}^{-2} \text{h}^{-1}$), suggesting that lipophilicity of molecules alters the transport rate through the mammary papilla. Due to the marginal surface area of the mammary ducts compared to the entire nipple cross-section, the difference in flux is likely attributable to the transepidermal transport contribution for SRB, for which the contribution of this transport route is minimal for NR. Furthermore, the partition coefficient (K), a thermodynamic parameter, is lower for NR (0.065 ± 0.026) than SRB (0.17 ± 0.035) indicating that NR is less able to penetrate the nipple compared to SRB. This is consistent with the fluorescence intensity profiles and the disposition kinetics presented in previous sections. Once NR penetrates the nipple, or overcomes the thermodynamic barrier, NR then diffuses more rapidly than SRB, which is evidenced by a higher diffusion coefficient for NR ($676,288 \pm 164,872 \mu\text{m}^2 \text{h}^{-1}$) than SRB ($390,919 \pm 58,770 \mu\text{m}^2 \text{h}^{-1}$) and a slightly shorter lag time (t_{lag}) for NR (16.5 h) than SRB (20.0 h). Dave et al. reported similar time lag (t_{lag}) and flux (J) trends through the nipple following permeation of the small molecules 5-fluorouracil and estradiol (Dave et al., 2014). In that study, the flux was smaller and lag time was shorter for the lipophilic molecule (estradiol) compared to the hydrophilic (5-fluorouracil) molecule.

3.4. Comparison of transpapillary and transdermal permeation kinetics

In order to further quantify the impact of transductal delivery, the permeation kinetics through porcine nipple were compared to the adjacent skin tissue. Using both tissue types allowed us to quantify kinetics through the transepidermal route alone (using skin) or through the combined transepidermal and transductal routes (using the nipple).

Both SRB and NR permeated quicker through trimmed skin compared to nipple, although the difference was not statistically significant for either fluorescent marker ($p = 0.290$ and $p = 0.697$ for SRB and NR, respectively) (Fig. 7). The cumulative amount of dye permeated through the skin reached 75.49 $\mu\text{g}/\text{cm}^2$ for SRB and 30.89 $\mu\text{g}/\text{cm}^2$ for NR, while through the nipple the values were 50.11 $\mu\text{g}/\text{cm}^2$ and 15.33 $\mu\text{g}/\text{cm}^2$ for SRB and NR, respectively. While we noted faster permeation through the skin than the nipple, Dave et al. (Dave et al., 2014) recently reported more rapid permeation through the nipple compared to skin. The variation in this trend can be at least partially explained by the difference in tissue thickness, as our skin specimens were 2.8-fold thinner than those used by Dave and coworkers. Differences in nipple height and specific location from which skin tissue was

Table 2

In vitro permeation parameters for NR and SRB through porcine nipple or skin.

Permeation parameter	Nipple		Skin	
	NR	SRB	NR	SRB
L (μm)	7350 \pm 350 [†]	6780 \pm 380 [†]	250 \pm 0 [†]	250 \pm 0 [†]
T_{lag} (h)	16.45 \pm 4.50	20.04 \pm 0.83	11.61 \pm 3.34	18.65 \pm 0.42
J ($\mu\text{g cm}^{-2} \text{h}^{-1}$)	0.47 \pm 0.11 [*]	1.71 \pm 0.35 [*]	0.81 \pm 0.25 [‡]	2.60 \pm 0.30 [†]
P ($\mu\text{m h}^{-1}$)	4.70 \pm 1.08	9.74 \pm 2.00	8.07 \pm 2.46	14.79 \pm 1.71
D ($\mu\text{m}^2 \text{h}^{-1}$)	676,288 \pm 164,872 [†]	390,919 \pm 58,770	1,169 \pm 472 [*]	559 \pm 12
K	0.065 \pm 0.026 [†]	0.17 \pm 0.035 [†]	1.87 \pm 0.35 ^{*,‡}	6.62 \pm 0.75 ^{*,‡}
r^2	0.90 \pm 0.054	0.98 \pm 0.0012	0.99 \pm 0.0031	0.99 \pm 0.0027

Mean \pm SEM.

Abbreviations: NR, nile red; SRB, sulforhodamine B; L, thickness of tissue; T_{lag} , lag time; J, flux; P, permeability coefficient; D, diffusion coefficient; K, partition coefficient; r^2 , goodness of fit.

^{*} Indicates significant difference ($p < 0.05$) in comparison to same dye, but different tissue.

[‡] Indicates significant difference ($p < 0.05$) in comparison to same tissue, but different dye.

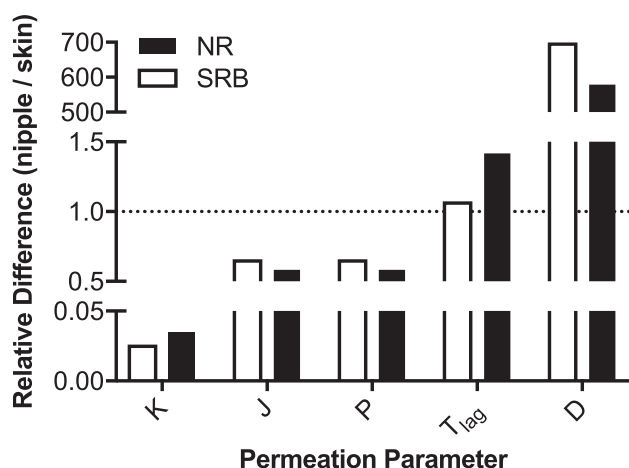


Fig. 8. Relative difference in permeation parameters between nipple and skin.

collected could also contribute to the variation, as well as the different detection methods used to quantify permeation.

The concomitant permeation parameters for transpapillary and transdermal permeation are listed in Table 2. Additionally, the relative difference between nipple and skin permeation parameters are shown in Fig. 8. Most of the permeation parameters, including lag time (T_{lag}), flux (J), and the permeation coefficient (P) are not statistically different between the skin and nipple. However, each of these parameters is highly dependent on tissue thickness (Cross et al., 2003), which differed greatly between the skin and nipple. As detailed in Table 2, the nipple tissue specimens were over 20 times thicker than the skin specimens used. The parameters that are normalized for tissue thickness (see equations in Materials & methods), specifically the diffusion coefficient (D) and partition coefficient (K), are statistically different when comparing the nipple to skin. For NR, the diffusion coefficient (D) is significantly ($p = 0.004$) higher through the nipple ($676,288 \pm 164,872 \mu\text{m}^2 \text{h}^{-1}$) than through the skin ($1,169 \pm 472 \mu\text{m}^2 \text{h}^{-1}$). For SRB, the diffusion coefficient is higher, though not significantly ($p = 0.091$), through the nipple ($390,919 \pm 58,770 \mu\text{m}^2 \text{h}^{-1}$) than through the skin ($559 \pm 12 \mu\text{m}^2 \text{h}^{-1}$). Based on the calculated diffusion coefficients (D), the relative difference in diffusivity through the nipple is 578-fold higher and 699-fold higher than through the skin for NR and SRB, respectively. These results further support the significant contribution of the mammary ducts in transpapillary transport for both fluorescent molecules. Because the nipple and skin are nonhomogeneous in structure, the calculated diffusion coefficients represent an effective diffusivity that approximates Fickian transport (Smith, 1990). However, this calculation is commonly used in Franz diffusion cell experiments with skin or other tissues (Mohd et al., 2016; Okamoto et al., 1988).

Meanwhile, the partition coefficient (K) is 0.026-fold lower and 0.035-fold lower through the nipple than skin for NR and SRB, respectively. The significant decrease in the partition coefficient is likely attributable to structural differences in the nipple's stratum corneum as compared to the skin, considering the stratum corneum is a primary barrier to drug penetration (Lawson et al., 2007).

4. Conclusions

The quantitative characterization of transport pathways through the nipple, as well as the associated penetration and permeation kinetics, in respect to a permeant's lipophilicity have been detailed here. Results from the fluorescence micrographs indicate two distinct penetration pathways: transepidermal, primarily used by hydrophilic molecules, and transductal, which is the primary transport pathway for lipophilic molecules. For the two model fluorescent dyes, retention within the tissue was largely impacted by the molecule's lipophilicity, while the

kinetics of permeation through the tissue was comparable irrespective of lipophilicity. This suggests that both molecule types capitalize on the mammary canals as a direct route through the nipple. This conclusion is further supported by the significantly higher diffusion coefficients for both dyes when comparing transpapillary to transdermal permeation. Using various levels of assessment, from micron-thick tissue sections to the analysis of the nipple as a whole, we have provided a thorough understanding of the fate of model dyes upon transpapillary drug delivery. These results reinforce the feasibility of this route of administration as a local, non-invasive approach for prevention and treatment of early stage breast cancer, or other breast diseases. Because of the relatively low molecular weight of the two model dyes, we expect that their permeation characteristics would be predictive of small molecular weight therapeutic drugs with similar lipophilic/hydrophilic properties. These results can also inform the design of appropriate delivery formulations optimized for transpapillary drug delivery. Future pre-clinical studies will focus on *in vivo* biodistribution and eventual establishment of therapeutic efficacy of transpapillary delivery of therapeutic drugs.

Funding

This work was supported by a Tulane University Carol Lavin Bernick Faculty Grant.

Acknowledgements

The authors of this study thank Anita Verdun of Verdun Farms Meat Market for providing porcine tissue used in our investigation.

References

- Alsharif, F.M., Dave, K., Samy, A.M., Saleh, K.I., Amin, M.A., Perumal, O., 2017. Influence of hydroalcoholic vehicle on *in vitro* transport of 4-hydroxy tamoxifen through the mammary papilla (Nipple). *AAPS PharmSciTech* 18, 1366–1373.
- Amato, D.V., Lee, H., Werner, J.G., Weitz, D.A., Patton, D.L., 2017. Functional microcapsules via thiol-ene photopolymerization in droplet-based microfluidics. *ACS Appl. Mater. Interfaces* 9, 3288–3293.
- American Cancer Society, 2016. *Cancer Facts & Figures 2015-2016*, Atlanta.
- American Cancer Society, 2017. *Cancer Facts and Figures 2017-18*, Atlanta.
- Cross, S.E., Magnusson, B.M., Winckle, G., Anissimov, Y., Roberts, M.S., 2003. Determination of the effect of lipophilicity on the *in vitro* permeability and tissue reservoir characteristics of topically applied solutes in human skin layers. *J. Invest. Dermatol.* 120, 759–764.
- Dave, K., Alsharif, F.M., Perumal, O., 2016. Transpapillary (Nipple) delivery of macromolecules to the breast: proof of concept study. *Mol. Pharm.* 13, 3842–3851.
- Dave, K., Averineni, R., Sahdev, P., Perumal, O., 2014. Transpapillary drug delivery to the breast. *PLoS One* 9, e115712.
- Davison, Z., 2008. *Transcutaneous Delivery of Anti-Breast Cancer Agents*. Cardiff University PhD thesis.
- Greenspan, P., Fowler, S.D., 1985. Spectrofluorometric studies of the lipid probe, Nile red. *J. Lipid. Res.* 26, 781–789.
- Hartmann, L.C., Degnim, A.C., Santen, R.J., Dupont, W.D., Ghosh, K., 2015. Atypical hyperplasia of the breast—risk assessment and management options. *N. Engl. J. Med.* 372, 78–89.
- Jaimes-Lizcano, Y.A., Lawson, L.B., Papadopoulos, K.D., 2011. Oil-frozen W(1)/O/W(2) double emulsions for dermal biomacromolecular delivery containing ethanol as chemical penetration enhancer. *J. Pharm. Sci.* 100, 1398–1406.
- Kim, S., Thiessen, P.A., Bolton, E.E., Chen, J., Fu, G., Gindulyte, A., Han, L., He, J., He, S., Shoemaker, B.A., Wang, J., Yu, B., Zhang, J., Bryant, S.H., 2016. PubChem substance and compound databases. *Nucl. Acids Res.* 44, D1202–1213.
- Kolliker, A., 2015. *Manual of Human Histology*. FB & C Limited.
- Kuchler, S., Abdel-Mottaleb, M., Lamprecht, A., Radowski, M.R., Haag, R., Schafer-Korting, M., 2009. Influence of nanocarrier type and size on skin delivery of hydrophilic agents. *Int. J. Pharm.* 377, 169–172.
- Lawson, L.B., Freytag, L.C., Clements, J.D., 2007. Use of nanocarriers for transdermal vaccine delivery. *Clin. Pharmacol. Ther.* 82, 641–643.
- Lee, L.M., Davison, Z., Heard, C.M., 2010. *In vitro* delivery of anti-breast cancer agents directly via the mammary papilla (nipple). *Int. J. Pharm.* 387, 161–166.
- Lee, O., Ivancic, D., Allu, S., Shidfar, A., Kenney, K., Helenowski, I., Sullivan, M.E., Muzzio, M., Scholtens, D., Chatterton, R.T., Bethke, K.P., Hansen, N.M., Khan, S.A., 2015. Local transdermal therapy to the breast for breast cancer prevention and DCIS therapy: preclinical and clinical evaluation. *Cancer Chemother. Pharmacol.* 76, 1235–1246.
- Lee, O., Page, K., Ivancic, D., Helenowski, I., Parini, V., Sullivan, M.E., Margenthaler, J.A., Chatterton, R.T., Jovanovic, B., Dunn, B.K., Heckman-Stoddard, B.M., Foster, K.,

- Muzzio, M., Shklovskaya, J., Skripkauskas, S., Kulesza, P., Green, D., Hansen, N.M., Bethke, K.P., Jeruss, J.S., Bergan, R., Khan, S.A., 2014. A randomized phase II pre-surgical trial of transdermal 4-hydroxytamoxifen gel versus oral tamoxifen in women with ductal carcinoma in situ of the breast. *Clin. Cancer Res.* 20, 3672–3682.
- Love, S.M., Barsky, S.H., 2004. Anatomy of the nipple and breast ducts revisited. *Cancer* 101, 1947–1957.
- Love, S.M., Zhang, W., Gordon, E.J., Rao, J., Yang, H., Li, J., Zhang, B., Wang, X., Chen, G., 2013. A feasibility study of the intraductal administration of chemotherapy. *Cancer Prev. Res. (Phila)* 6, 51–58.
- Mannhold, R., Poda, G.I., Ostermann, C., Tetko, I.V., 2009. Calculation of molecular lipophilicity: State-of-the-art and comparison of log P methods on more than 96,000 compounds. *J. Pharm. Sci.* 98, 861–893.
- Martineau, G.-P., Farmer, C., Peltoniemi, O., 2012. *Diseases of Swine*, 10 ed. John Wiley & Sons Inc.
- Mohd, F., Todo, H., Yoshimoto, M., Yusuf, E., Sugibayashi, K., 2016. Contribution of the hair follicular pathway to total skin permeation of topically applied and exposed chemicals. *Pharmaceutics* 8.
- Okamoto, H., Hashida, M., Sezaki, H., 1988. Structure-activity relationship of 1-alkyl- or 1-alkenylazacycloalkanone derivatives as percutaneous penetration enhancers. *J. Pharm. Sci.* 77, 418–424.
- Schneider, C.A., Rasband, W.S., Eliceiri, K.W., 2012. NIH Image to ImageJ: 25 years of image analysis. *Nat. Methods.* 9, 671–675.
- Smith, K.L., 1990. Penetrant Characteristics Influencing Skin Absorption. In: Kempainen, B.W., Reifenrath, W.G. (Eds.), *Methods for Skin Absorption*. CRC Press, Boca Raton, pp. 23–34.
- Smith, S.G., Sestak, I., Forster, A., Partridge, A., Side, L., Wolf, M.S., Horne, R., Wardle, J., Cuzick, J., 2016. Factors affecting uptake and adherence to breast cancer chemoprevention: a systematic review and meta-analysis. *Ann. Oncol.* 27, 575–590.
- Tan, G., Xu, P., Lawson, L.B., He, J., Freytag, L.C., Clements, J.D., John, V.T., 2010. Hydration effects on skin microstructure as probed by high-resolution cryo-scanning electron microscopy and mechanistic implications to enhanced transcutaneous delivery of biomacromolecules. *J. Pharm. Sci.* 99, 730–740.
- Yan, D., Lu, J., Wei, M., Evans, D.G., Duan, X., 2009. Sulforhodamine B intercalated layered double hydroxide thin film with polarized photoluminescence. *J. Phys. Chem. B* 113, 1381–1388.
- Yu, B., Dong, C.Y., So, P.T., Blankschtein, D., Langer, R., 2001. In vitro visualization and quantification of oleic acid induced changes in transdermal transport using two-photon fluorescence microscopy. *J. Invest. Dermatol.* 117, 16–25.